
Root Cause Analysis of Outliers in Unknown Cyclic Graphs

Daniela Schkoda^{1, 2}

Dominik Janzing¹

¹Amazon Research, Tübingen, Germany

²TUM School of Computation, Information and Technology, Munich, Germany

Abstract

We study the propagation of outliers in cyclic causal graphs with linear structural equations, tracing them back to one or several “root cause” nodes. We show that it is possible to identify a short list of potential root causes provided that the perturbation is sufficiently strong and propagates according to the same structural equations as in the normal mode. This short-list consists of the true root causes together with those of its parents lying on a cycle with the root cause. Notably, our method does not require prior knowledge of the causal graph.

1 Introduction

Root cause diagnosis is a fundamental challenge across a wide range of domains. Whether tracing the origin of a failure in a cloud-based microservice architecture, identifying a perturbed gene in a gene-regulatory network, locating the source of a shock in a financial system, or detecting faults in industrial manufacturing processes, the need to accurately pinpoint the source of disruptions is critical. For instance, in microservice-based cloud applications, when a failure occurs in one service, its effects can propagate across others, creating a cascade of symptoms and thousands of alerts. Root cause analysis (RCA) is thus critical for maintaining reliability and availability.

RCA closely aligns with the task of intervention targets estimation (ITE). While the framing differs slightly, in both cases, interventions on a few nodes in a causal system explain shifts in the overall distribution, and the goal is to identify these nodes.

Existing methods for both tasks largely fall into two categories. The first one includes graph-based methods,

which require (or first learn) a ground truth causal graph (Kim et al., 2013; Assaad et al., 2023; Tao et al., 2024; Xie et al., 2024; Tonon et al., 2025). However, in practice, obtaining a complete ground-truth model for large systems is typically infeasible, and causal discovery methods to learn them from data often rely on restrictive and unverifiable assumptions. To address this, a second line of work performs RCA without relying on a known ground truth: For instance, Ikram et al. (2022) only partially reconstructs the underlying graph to effectively identify root causes, while Shan et al. (2019) leverages time series data for root cause detection. Varici et al. (2021, 2022); Wang et al. (2018); Ghoshal et al. (2019); Malik et al. (2024) learn the intervention targets by inspecting the difference of the precision matrices of the observational and interventional data and Yang et al. (2024) by applying contrastive learning to recover exogenous noises that shift between both data sets.

A shared limitation across all these works is the reliance on multiple anomalous samples. In contrast, Okati et al. (2025) introduce two RCA approaches that operate with only a single anomalous sample: *Smooth Traversal*, which again requires ground-truth knowledge of the causal DAG (but not of the conditional distributions or even SCMs), and *Score Ordering*, which avoids such knowledge but assumes that the unknown ground truth follows a polytree structure. The work most closely related to ours is Li et al. (2024), which assumes a linear structural equation model (SEM) and demonstrates that a permutation search combined with Cholesky decomposition of the covariance matrix can uncover the root cause, even in the case of a single interventional sample. However, their approach still requires an *acyclic* ground-truth structure, which is again often violated in practice: gene regulatory networks routinely contain cyclic feedback loops, and microservice calls can form cycles, e.g., through repeated calls after failures (Genfer and Zdun, 2021; Sedghpour et al., 2023).

In this work, we address exactly this gap. We consider the task of root cause analysis in settings described by SEMs that may include cycles without requiring ground truth. Our approach is heavily inspired by Li et al. (2024) as it also uses the covariance matrix to derive a simple linear transformation that reveals root causes when applied to the vector of outlier observations. However, it is conceptually more straightforward and avoids the expensive combinatorial search needed there, making it more computationally efficient; see the appendix for a more detailed comparison of the ideas.

2 Notation and Model

Our method assumes access to data under the normal regime, along with one anomalous sample for which we seek to identify the root causes of the abnormality. We model the p -variate distribution under the normal regime, denoted by P^X , using a linear cyclic SEM (Richardson, 1996; Spirtes et al., 2001; Bongers et al., 2021). Specifically, each feature X_i of $X = (X_1, \dots, X_p)$ satisfies

$$X_i = \sum_{j=1}^p a_{ij} X_j + N_i, \quad (1)$$

or, in matrix-vector-form,

$$X = AX + N, \quad (2)$$

where A is a coefficient matrix with zero diagonal entries, and N is a noise vector with mean zero and uncorrelated components¹. We further assume that $I - A$ is invertible. The matrix A defines the system’s causal structure, with a non-zero entry a_{ij} indicating a direct causal effect from variable X_j to variable X_i . This structure is naturally represented by a directed graph \mathcal{G} , where an edge $X_j \rightarrow X_i$ exists if and only if $a_{ij} \neq 0$. We assume that the same linear relations still hold in the anomalous mode up to a sparse additive perturbation term Δ :

$$\tilde{x} = A\tilde{x} + n + \Delta, \quad (3)$$

where n is an i.i.d. copy of N and Δ has non-zero entries for the root cause nodes, which we denote by \mathcal{R} . We may also absorb the perturbation into the noise² by defining $\tilde{n} = n + \Delta$. With this notation, the task

¹Unlike many works in causal discovery, we do not require the noise terms to be mutually independent; uncorrelatedness suffices.

²Modelling the perturbation as a change of the noise does not mean that we assume a perturbation affecting the exogenous noise in any “material” sense. For example, assume that the root cause manifests as a change in the causal mechanisms, $\tilde{x}_r = f(\text{pa}(r), \tilde{n}_r)$, whereas in the normal mode, $X_r = \sum_{i \in \text{pa}(r)} a_{ri} X_i + n_r$. This modification

of RCA lies in identifying which entries of the noise vector in \tilde{n} are extreme when compared to the original noise vector N . To make the connection between X and N more explicit, we can rearrange (2) as

$$X = (I - A)^{-1}N.$$

The entries of $(I - A)^{-1}$ capture *total causal effects* and are related to paths in the graph \mathcal{G} . A *path* from i_1 to i_k , denoted by $i_1 \rightsquigarrow i_k$, is a sequence of edges $(i_1 \rightarrow i_2, i_2 \rightarrow i_3, \dots, i_{k-1} \rightarrow i_k)$ such that neither nodes nor edges are repeated, except possibly for a return to the starting node, $i_1 = i_k$, forming a cycle. We allow paths of length 0. The following standard result will become important later:

Lemma 2.1 (Path matrix). *The total causal effect from j on i multiplies direct causal effects along paths from j to i :*

$$((I - A)^{-1})_{ij} = \frac{1}{\det(I - A)} \sum_{\pi: j \rightsquigarrow i} \prod_{k \rightarrow h \in \pi} a_{hk} \cdot \left(1 + \sum_{\substack{(C_1, \dots, C_q) \in \mathcal{C}_\pi, \\ q \geq 1}} (-1)^q \prod_{m=1}^q \prod_{k \rightarrow h \in C_q} a_{hk} \right),$$

where $\mathcal{C}_\pi = \{(C_1, \dots, C_q) : \text{collection of disjoint cycles in } \tilde{\mathcal{G}} \text{ not using any node in } \pi; q \in \mathbb{N}_0\}$.

While the proof is provided in the supplementary material, especially for acyclic graphs, the intuition is quite straightforward: the total causal effect accounts for all paths - direct and indirect - through which one variable can influence another. Each path represents a potential causal route, and its contribution is the product of the direct effects along it. This motivates to call $(I - A)^{-1}$ the *path matrix*. As our primary interest lies in the sparsity pattern of the matrix, we omit the explicit determinant formula here and refer the reader to the proof of Lemma 4.5 in Amendola et al. (2020).

Many of the results proven in this paper assume *genericity* of the parameters A and Σ_{NN} , meaning that the results might fail on a Lebesgue measure zero set of matrices A (consistent with a fixed graph G) and choices of Σ_{NN} . This assumption rules out degenerate cases, such as interventions on two nodes that cancel each other. For example, in the chain

$$X_1 \rightarrow X_2 \rightarrow X_3$$

can be “absorbed” into a perturbation term δ such that it matches our framework: $\tilde{x}_r = \sum_{i \in \text{pa}(r)} a_{ri} X_i + n_r + \delta$, where $\delta = f(\text{pa}(r), \tilde{n}_r) - \sum_{i \in \text{pa}(r)} a_{ri} X_i - n_r$; compare also Von Kügelgen et al. (2023).

with all edge weights being one and two root causes X_1, X_2 with $\delta_1 = 1, \delta_2 = -1$, we obtain $\tilde{x}_2 = n_1 + n_2 + \delta_1 + \delta_2 = n_1 + n_2$, which is not anomalous although X_2 is a root cause. Our method cannot identify X_2 as the root cause in this pathological case. A precise characterization of these exceptional situations, as well as most proofs, are deferred to the appendix. Finally, we denote the children, parents, descendants, and ancestors of a node X_i by $\text{ch}(X_i), \text{pa}(X_i), \text{de}(X_i)$, and $\text{an}(X_i)$, respectively.

Having established the model, we discuss how Root Cause Analysis can be solved in this framework.

3 Root Cause Analysis via Invariant Structural Equations

3.1 Causally Sufficient Cyclic Model

We first consider the case of a single root cause, that is $\Delta = (0, \dots, 0, \delta, 0, \dots, 0)$ with $\delta \in \mathbb{R}$ representing a significant perturbation at the root cause r . A key ingredient of our method is the precision matrix, which can be conveniently expressed in terms of the path matrix. Specifically,

$$\Sigma_{XX} = (I - A)^{-1} \Sigma_{NN} (I - A)^{-T},$$

where Σ_{NN} denotes the covariance matrix of the noise, which is diagonal by assumption: $\Sigma_{NN} = \text{diag}(\sigma_1^2, \dots, \sigma_p^2)$. Inverting this expression yields the precision matrix:

$$\Theta_{XX} := \Sigma_{XX}^{-1} = (I - A)^T \Theta_{NN} (I - A),$$

where Θ_{NN} denotes the precision matrix of N . To build intuition for how this relationship informs root cause analysis, we first consider a simple two-dimensional toy example.

Example 1. Assume the data-generating process is described by the causal DAG $X_1 \rightarrow X_2$, and both X_1 and X_2 are standard normally distributed. The structural equations are

$$\begin{aligned} X_1 &= N_1, \\ X_2 &= \rho X_1 + N_2, \end{aligned}$$

where ρ denotes the Pearson correlation between X_1 and X_2 . Further, the covariance matrix and its inverse read

$$\Sigma_{XX} = \begin{pmatrix} 1 & \rho \\ \rho & 1 \end{pmatrix}, \quad \Theta_{XX} = \frac{1}{1 - \rho^2} \begin{pmatrix} 1 & -\rho \\ -\rho & 1 \end{pmatrix}.$$

If X_1 is the root cause, i.e., $\Delta = (\delta, 0)^T$, the unperturbed vector x is moved to $\tilde{x} = x + (\delta, \delta \cdot \rho)^T$. Applying Θ_{XX} to \tilde{x} yields

$$\Theta_{XX} \tilde{x} = \Theta_{XX} x + \Theta_{XX} \delta \begin{pmatrix} 1 \\ \rho \end{pmatrix} = \Theta_{XX} x + \begin{pmatrix} \delta \\ 0 \end{pmatrix},$$

where only the first entry is extreme for $\delta \rightarrow \infty$. On the other hand, if X_2 is the root cause, we have $\Delta = (0, \delta)^T$ and $\tilde{x} = x + (0, \delta)^T$ and obtain

$$\begin{aligned} \Theta_{XX} \tilde{x} &= \Theta_{XX} x + \Theta_{XX} \begin{pmatrix} 0 \\ \delta \end{pmatrix} \\ &= \Theta_{XX} x + \delta \cdot \frac{1}{1 - \rho^2} \begin{pmatrix} -\rho \\ 1 \end{pmatrix}, \end{aligned}$$

where both entries of the vector get extreme for high δ , hence we can tell the difference between the two scenarios.

To see how this idea generalizes, set $\xi = \Theta_{XX} \tilde{x}$ and obtain $\xi = \Theta_{XX} \tilde{x} = \Theta_{XX} (I - A)^{-1} (\Delta + n)$. Inspecting the first summand, we observe

$$\begin{aligned} \Theta_{XX} (I - A)^{-1} \Delta &= (I - A)^T \Theta_{NN} (I - A) (I - A)^{-1} \Delta \\ &= (I - A)^T \Theta_{NN} \Delta \\ &= \frac{1}{\sigma_r^2} \delta (I - A)^T e_r =: \xi' \end{aligned} \quad (4)$$

Since the r th column of $(I - A)^T$ is non-zero precisely at the positions of r and its parents, also ξ' is non-zero only at these positions. Turning to the second summand, $\Theta_{XX} (I - A)^{-1} n$, note that it has the same distribution as $\Theta_{XX} X$ since $n \stackrel{d}{=} N$. Therefore, by evaluating which ξ_i has the same distribution as $\Xi_i := (\Theta_{XX} X)_i$, we can separate the root cause and its parent from the remaining nodes. Especially, if δ has high absolute value, we can expect the entries of the root cause and its parents to differ significantly from all other entries. Overall, we derived:

Applying the precision matrix to the outlier vector leaves only the root causes and their parents as extreme, thereby revealing them.

Theorem 3.1 (Shortlist of root causes). For generic A and Σ_{NN} , all entries in ξ_i follow their usual distribution, except the root causes and potentially their parents:

$$\mathcal{R} \subseteq \{\xi_i \stackrel{d}{\neq} \Xi_i\} \subseteq \mathcal{R} \cup \text{pa}(\mathcal{R}).$$

This result gives a first short list of candidate root causes. To restrict the list further, we can make use of the fact that only the descendants of the root causes are anomalous.

Theorem 3.2 (Even shorter list of root causes). *Assuming generic parameters A, Σ_{NN} , an abnormal distribution of both, ξ and \tilde{x} , occurs only for the root cause and for its parents that are simultaneously descendants:*

$$\mathcal{R} \subseteq \{\xi_i \stackrel{d}{\neq} \Xi_i \text{ and } \tilde{x}_i \stackrel{d}{\neq} X_i\} \subseteq \mathcal{R} \cup (\text{pa}(\mathcal{R}) \cap \text{de}(\mathcal{R})).$$

Note that Theorem 3.2 allows for unique identification of the root cause (if there is only one) in acyclic graphs as the parents of the root cause cannot be descendants at the same time.

Another challenge is dealing with latent variables – factors that influence the system but are not measured.

3.2 Latent Cyclic Model

Latent variables can be incorporated into the model by extending the variable set. We consider a random vector $Z = (X, L)$, where $X = (X_1, \dots, X_p)$ collects the observed variables and $L = (L_1, \dots, L_q)$ the latent variables. Overall, Z captures all variables relevant to the underlying causal system and satisfies a linear SEM

$$Z = AZ + N \quad \text{and} \quad \tilde{z} = A\tilde{z} + n + \Delta, \quad (5)$$

which can be partitioned as

$$\begin{pmatrix} X \\ L \end{pmatrix} = \begin{pmatrix} A_{XX} & A_{XL} \\ A_{LX} & A_{LL} \end{pmatrix} \begin{pmatrix} X \\ L \end{pmatrix} + \begin{pmatrix} N_X \\ N_L \end{pmatrix},$$

similarly for the interventional equation. We aim to express the system in terms of X only, by incorporating the latent components into the noise term, at the cost of losing noise uncorrelatedness. To this end, denote

$$S = A_{XX} + A_{XL}(I - A_{LL})^{-1}A_{LX},$$

and let D the diagonal matrix of the same shape with entries $d_{ii} = \frac{1}{1-s_{ii}}$. Further define

$$\begin{aligned} \bar{A}_{ij} &= (DS)_{ij} \text{ for } i \neq j, \text{ and } 0 \text{ otherwise,} \\ \bar{N} &= D(N_X + A_{XL}(I - A_{LL})^{-1}N_L), \\ \bar{\Delta} &= D(\Delta_X + A_{XL}(I - A_{LL})^{-1}\Delta_L). \end{aligned}$$

Lemma 3.3 (Remove nodes). *If P^Z satisfies the SEM (5), then P^X and $P^{\tilde{x}}$ fulfill*

$$X = \bar{A}X + \bar{N} \quad \text{and} \quad \tilde{x} = \bar{A}\tilde{x} + \bar{n} + \bar{\Delta}.$$

Proof. We show the observational SEM; the interventional one works analogously. As a first step, we prove

that $X = SX + M$, where $M = N_X + A_{XL}(I - A_{LL})^{-1}N_L$. Note that

$$I - S = ((I - A_{XX}) - A_{XL}(I - A_{LL})^{-1}A_{LX})$$

is precisely the Schur complement (Schur, 1917) of the block $I - A_{LL}$ in $I - A$, yielding that

$$((I - A)^{-1})_{XX} = (I - S)^{-1},$$

and,

$$((I - A)^{-1})_{XL} = (I - S)^{-1}A_{XL}(I - A_{LL})^{-1}.$$

Combining both yields

$$\begin{aligned} (I - S)^{-1}M &= ((I - A)^{-1})_{XX}N_X \\ &\quad + (I - S)^{-1}A_{XL}(I - A_{LL})^{-1}N_L \\ &= ((I - A)^{-1})_{XX}N_X + ((I - A)^{-1})_{XL}N_L \\ &= X, \end{aligned}$$

which confirms the intermediate equation system for X . While this representation accurately describes X , it does not yet constitute a valid SEM since S may feature non-zero diagonal entries. To enforce zero diagonals, we apply a rescaling. Writing out the i -th component,

$$X_i = a'_{ii}X_i + \sum_{j \neq i} a'_{ij}X_j + M_i,$$

then subtracting $a'_{ii}X_i$, and rescaling both sides gives the SEM stated in the lemma:

$$X_i = \frac{1}{1 - a'_{ii}} \left(\sum_{j \neq i} a'_{ij}X_j + M_i \right).$$

□

Example 2. *For the SEM depicted in Figure 1a, that is,*

$$\begin{pmatrix} X_1 \\ X_2 \\ X_3 \\ L_1 \\ L_2 \end{pmatrix} = \begin{pmatrix} 0 & 0 & 0 & a_{14} & 0 \\ 0 & 0 & 0 & 0 & a_{25} \\ a_{31} & a_{32} & 0 & a_{34} & 0 \\ 0 & 0 & 0 & 0 & 0 \\ a_{51} & 0 & 0 & 0 & 0 \end{pmatrix} \begin{pmatrix} X_1 \\ X_2 \\ X_3 \\ L_1 \\ L_2 \end{pmatrix} + \begin{pmatrix} N_1 \\ N_2 \\ N_3 \\ N_4 \\ N_5 \end{pmatrix}$$

the projected SEM, visualized in Figure 1b, reads

$$\begin{pmatrix} X_1 \\ X_2 \\ X_3 \end{pmatrix} = \begin{pmatrix} 0 & 0 & 0 \\ a_{25}a_{51} & 0 & 0 \\ a_{31} & a_{32} & 0 \end{pmatrix} \begin{pmatrix} X_1 \\ X_2 \\ X_3 \end{pmatrix} + \begin{pmatrix} N_1 + a_{14}L_1 \\ N_2 + a_{25}L_2 \\ N_3 + a_{34}L_3 \end{pmatrix}.$$

Here, each latent variable is absorbed into the noise terms of its children, making the noises of nodes with a common latent parent correlated. Moreover, removing L_2 from the system introduces a direct link $X_1 \rightarrow X_2$, reflecting what was previously an indirect, mediated path.

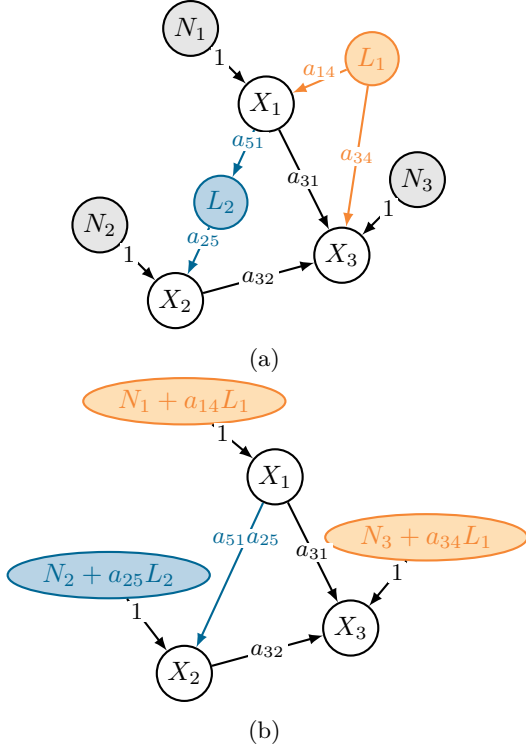


Figure 1: Projecting a linear SEM to an SEM for only the observed nodes.

In general graphs, \bar{N}_i and \bar{N}_j are correlated whenever they have a joint latent ancestor that connects to both through a path in which all inner nodes are latent, called *latent path* henceforth, and represented by $Z_k \rightsquigarrow \dots \rightsquigarrow Z_l$. Similarly, $\bar{\Delta}_i \neq 0$ for all observed root causes and all i which lie downstream of a latent root cause through a path consisting only of latent nodes. We refer to all these nodes i as *observable root causes*, aligning with the intuition that we cannot identify a root cause that was never observed. Instead, the observable root causes are the earliest observed nodes infected by the anomalies.

From the projected SEM over X , the precision matrix can be computed as:

$$(\Sigma_{XX})^{-1} = (I - \bar{A})^T (\Sigma_{\bar{N}\bar{N}})^{-1} (I - \bar{A}).$$

In contrast to the case without latent variables, the noise precision matrix $(\Sigma_{\bar{N}\bar{N}})^{-1}$ is not necessarily diagonal due to correlations introduced by marginalizing out latent nodes. Instead, its sparsity pattern can be described as follows.

Lemma 3.4 (Sparse noise precision matrix). $(\Theta_{\bar{N}\bar{N}})_{ij} = 0$ if there exists no sequence of latent paths

$$X_i \leftarrow \dots \leftarrow L_{l_1} \rightsquigarrow \dots \rightsquigarrow X_{k_1} \leftarrow \dots \leftarrow L_{l_2} \rightsquigarrow \dots \rightsquigarrow X_{k_2} \leftarrow \dots \rightsquigarrow X_j,$$

with $l_l \in [q], k_l \in [p]$.

Following Boege et al. (2025), we call such sequences of paths *zig-zag-structures* and denote them by $X_i \rightsquigarrow \dots \rightsquigarrow X_j$. For example, for $G = X_1 \leftarrow L_1 \rightarrow X_2 \leftarrow L_2 \rightarrow X_3$,

$$\bar{N} = \begin{pmatrix} N_1 + a_{14}L_1 \\ N_2 + a_{24}L_1 + a_{25}L_2 \\ N_3 + a_{35}L_2 \end{pmatrix}.$$

While \bar{N}_1 and \bar{N}_3 are marginally independent, conditioning on \bar{N}_2 introduces dependence.

As before, we define the score vector as

$$\begin{aligned} \xi &= \Theta_{XX} \tilde{x} \\ &= (I - \bar{A})^T \Theta_{\bar{N}\bar{N}} \bar{\Delta} + (\Sigma_{XX})^{-1} (I - \bar{A})^{-1} \bar{n} \end{aligned}$$

Since the first term dominates for large perturbations, we are again interested in its support. From the Lemma, $\Theta_{\bar{N}\bar{N}} \bar{\Delta}$ is non-zero for all X_j having a zig-zag-connection to an observable root cause. Furthermore, \bar{A} encodes the child-parent relationships in the projected graph, that is, $a_{ij} \neq 0$ if and only if $X_j \rightsquigarrow \dots \rightsquigarrow X_i$.

Theorem 3.5 (Shortlist of root causes). *If A and Σ_{NN} are generic, then $\xi_i \neq 0$ if and only if X_i is connected to an observable root cause X_k through the structure*

$$X_i \rightsquigarrow \dots \rightsquigarrow X_j \rightsquigarrow \dots \rightsquigarrow X_k.$$

As before, this shortlist can be restricted further by removing non-anomalous nodes. Besides the obvious application of RCA in systems including latent variables, this theory also enables tracing the routes through which anomalies propagate.

Example 3 (Find root cause propagation route). *Assume again G is causally sufficient and X_r is identified as the unique root cause. A natural next step is identifying which nodes were subsequently affected, i.e., infer the children of X_r . To this end, we remove X_r from the data and look at $\xi_{\hat{r}}$. From Theorem 3.5, this is non-zero precisely at the positions i where there is a route*

$$X_i \rightsquigarrow \dots \rightsquigarrow X_j \rightsquigarrow \dots \rightsquigarrow X_k \leftarrow \dots \leftarrow X_r.$$

Since X_r is the sole latent node in this setting, this collapses to X_j being a child of X_r and $X_i = X_j$, or X_i being a parent of X_r or X_j . So, again, we have a candidate set for the children. Reiterating this approach, we can find supersets of all routes through which the anomaly propagated.

4 Implementation with False Discovery Rate Control (FDRC)

Turning to the practical implementation, we assume to have access to one anomalous sample \tilde{x} , alongside m i.i.d samples $X^{(1)}, \dots, X^{(m)} \sim P^X$, collected into a data matrix $\mathbf{X} \in \mathbb{R}^{m \times p}$. We first focus on Theorems 3.1 and 3.5, which identify candidate root causes as the nodes that violate the hypothesis

$$H_0 : \xi_i \stackrel{d}{=} \Xi_i.$$

For simplicity, we henceforth refer to these violating nodes as *positive*, while the others are termed *negative*. A straightforward approach to assess H_0 is to use the empirical p-value, defined as the proportion of samples $|\Xi_i|$ exceeding $|\xi_i|$. While this guarantees valid Type I error control for incorrectly classifying a *single* negative node as positive, it is challenging to use p-values with arbitrary dependencies to control the total number of false positives within a False Discovery Rate Control (FDRC) framework. Therefore, we instead turn to *e-values*, where an e-value is a non-negative random variable e satisfying $\mathbb{E}(e) \leq 1$ under H_0 . High values of e indicate stronger evidence against the null hypothesis. Unlike p-values, e-values are particularly well-suited for multiple testing and aggregation, making them effective for FDRC; see Vovk and Wang (2021); Grünwald et al. (2024) for further details. In our setting,

$$e_i = \frac{\xi_i^2}{(\Theta_{XX})_{ii}} \quad (6)$$

is a valid e-value since under H_0 , ξ_i is centered and has covariance $(\Theta_{XX})_{ii}$, implying $\mathbb{E}(e) = 1$. Note that this e-value coincides with a commonly used outlier score, namely the squared Z-score defined via

$$\text{Z-score}(\xi_i; \Xi_i)^2 = \left(\frac{\xi_i - \mu_{\Xi_i}}{\sigma_{\Xi_i}} \right)^2.$$

The equivalence follows from the fact that Ξ is centered and has covariance $\Sigma_{\Xi\Xi} = \Theta_{XX}$. Following the e-value based FDRC approach introduced in Wang and Ramdas (2022), we denote by $e_{[1]}, \dots, e_{[p]}$ the e-values e_1, \dots, e_p arranged in decreasing order and obtain:

Lemma 4.1 (Benjamini-Hochberg for e-values). *Let $\alpha > 0$ be a desired FDR control level and define k^* as the largest index k such that $ke_{[k]} \geq 1/\alpha$. Then, selecting the k^* nodes corresponding to $e_{[1]}, \dots, e_{[k^*]}$ as candidate root causes yields*

$$\text{FDR} = \mathbb{E} \left(\frac{\text{false positives}}{\text{total number of rejections}} \right) \leq \alpha.$$

where the expectation is over the variables $X^{(1)}, \dots, X^{(n)} \sim P^X, \tilde{x} \sim P^{\tilde{x}}$. Finally, to incorporate the fact that the root cause is anomalous as stated in Theorem 3.2, we assign a root cause score of zero to all nodes not qualifying as outliers, as measured by their squared Z-scores falling below a threshold τ . The resulting procedure is summarized in Algorithm 1. The computational complexity of our algorithm breaks

Algorithm 1 Cyclic RCA

Require: Normal samples $\mathbf{X} \in \mathbb{R}^{m \times p}$, anomalous sample $\tilde{x} \in \mathbb{R}^p$, threshold τ to characterize outliers.

- 1: $\hat{\Theta} \leftarrow$ estimated precision matrix of \mathbf{X} .
- 2: $\hat{\xi} \leftarrow \hat{\Theta}\tilde{x}$.
- 3: $\hat{\Xi} \leftarrow \hat{\Theta}\mathbf{X}$
- 4: **for** $i = 1$ to p **do**
- 5: $s_i \leftarrow \text{Z-score}(\xi_i; \Xi_i)^2$
- 6: **if** $\text{Z-Score}(\tilde{x}; X)^2 < \tau$ **then**
- 7: $s_i \leftarrow 0$.
- 8: **return** RCA scores $s = (s_1, \dots, s_p)$.

down to its bottleneck: estimation of the precision matrix. Using Graphical Lasso (Friedman et al., 2008) incurs a cost of $O(Tp^3)$, where T is the iteration limit. A simpler option is to invert the sample covariance, with complexity $O(mp^2 + p^3)$. In both cases, space complexity is $O(mp + p^2)$. Further estimation methods are discussed in Appendix D.2.

Beyond the linear algebra formulation presented here, our method admits alternative (but slightly more involved) derivations, provided in appendix B. One such view links our score $\text{Z-score}(\xi_i; \Xi_i)$ to linear regression. Furthermore, under certain assumptions, our null hypothesis $\xi_i \stackrel{d}{=} \Xi_i$ can be rephrased as a conditional independence test, after introducing a binary indicator variable distinguishing anomalous from normal samples. This perspective clarifies the relation to conditional independence-based RCA (Kocaoglu et al., 2019; Jaber et al., 2020; Mooij et al., 2020; Ikram et al., 2022), while also highlighting a key difference: owing to our parametric assumptions, we can perform the test with only a single anomalous sample.

5 Experiments

More details on the experiments, the entailed statistical challenges, and further simulation studies can be found in the appendix. All experiments were executed on a MacBook Pro (Apple M1, 36 GB RAM) or an internal cluster with 80 logical cores and 754 GB RAM.

5.1 Simulation Studies

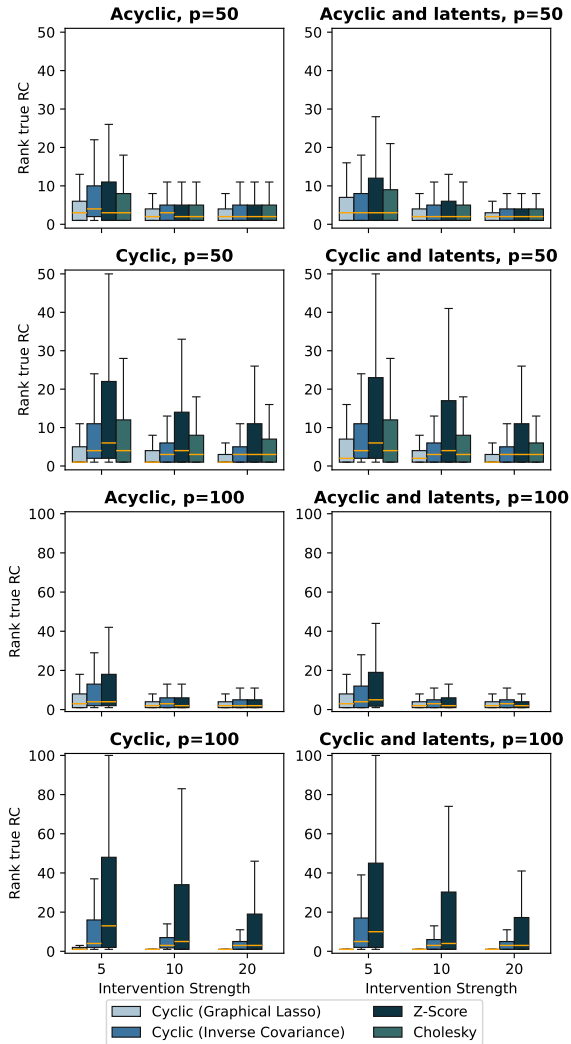


Figure 2: The boxplots illustrate the rank of the true root cause score among the scores of all nodes. Cyclic (Graphical Lasso) achieves the strongest performance, whereas Cyclic (Inverse Covariance) performs comparably to Cholesky. As expected, Z-Score yields the weakest results. Results for Cholesky with $p = 100$ are omitted due to computational infeasibility.

We evaluate our approach by comparing it to the method proposed in Li et al. (2024), which, to our knowledge, is the only method that works for DAGs and neither requires a ground truth graph nor multiple anomalous samples. Additionally, we include a Z-score baseline, which directly uses $Z\text{-score}(x_i; \mathbf{X}_i)^2$ as root cause score.³ In the Graphical Lasso variant of our

³This technique simply ranks nodes by their anomalousness and has been referred to as baseline Li et al. (2024). It offers theoretical guarantees for detecting the actual root cause only for collider-free polytrees. Nevertheless, some

Table 1: Means and standard deviations of the compute times in seconds for all methods. Cyclic (G) indicates Cyclic (Graphical Lasso) and (I) Inverse Covariance.

Method	Compute time	
	50 nodes	100 nodes
Cyclic (G)	3.44±2.61	993.07±463.90
Cyclic (I)	0.25±0.13	2.55±0.83
Z-Score	0.01±0.02	0.03±0.05
Cholesky	572.80±234.58	3676.38±2044.36

algorithm, we set the regularization parameter to 0.1.

To generate data, we first simulate graphs with 50 or 100 observed nodes across four settings: cyclic or acyclic, each either with or without five additional latent nodes. Edges are sampled independently at random with a probability calibrated such that the expected node degree is 3. Given the graph, data with $m = 10 \cdot p$ is synthetically generated via the corresponding linear SEM, where the non-zero entries of the coefficient matrix B are uniformly sampled from $[-2, -0.5] \cup [0.5, 2]$. Noise follows one of four distributions (Gaussian, uniform, exponential, lognormal). The number of root causes varies between 1 and 4, and intervention strength δ ranges from 5 to 20.

Figure 2 reports the aggregated results across all noise distributions and numbers of root causes. Each box summarizes 400 replications with varying random seeds. The median is indicated by the yellow line, the box represents the interquartile range (IQR), and the whiskers extend to 1.5 times the IQR. Table 1 shows the corresponding compute times. Cyclic (Graphical Lasso) is both more accurate and about four times faster than Cholesky. Cyclic (Inverse Covariance) matches Cholesky in accuracy but is substantially faster. Detailed breakdowns by noise type and number of root causes, as well as experiments with varying expected node degree and semi-synthetic data, are deferred to the appendix.

5.2 Cloud Computing Performance Metrics

For a case study on real-world data, we use the Pet-Shop datasets (Hardt et al., 2024), which comprise four benchmark datasets designed for evaluating RCA methods in microservice-based applications. Each contains latency, request, and availability metrics of 41

justification for inferring highly scored nodes as root cause candidates has been provided by Okati et al. (2025) when scores are obtained from p-values.

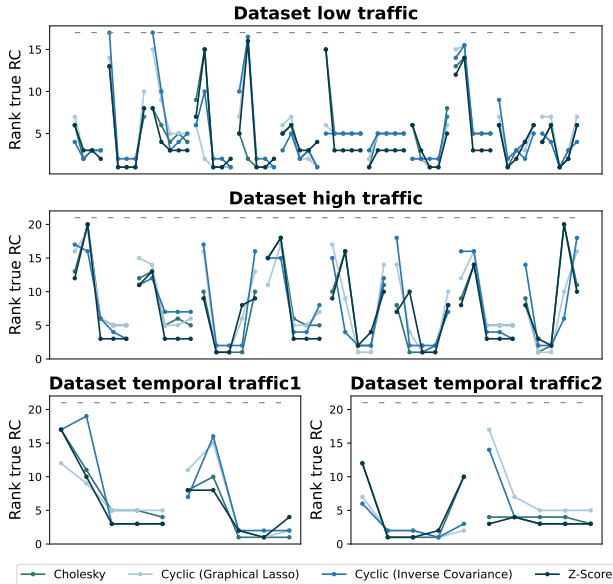


Figure 3: The rank of the true root cause’s score is shown, with the dotted line indicating the total number of services. The dots connected by lines belong to the same incident. Notably, all methods show similar performance, which is often poor at the beginning and occasionally at the end of each incident, while it improves in the middle. This could stem from a time gap between the incident triggering and its impact on the system and a potential resolution by the end. Indeed, at the beginning and the end, the true root cause is often not even anomalous; compare the appendix for details. In contrast, at the middle time points, the root causes often have very high outlier scores, which is probably why the Z-Score baseline performs quite well.

services collected at 5-minute intervals, alongside several injected performance issues at different services. These issues last approximately half an hour, yielding multiple interventional samples per incident. Due to challenges such as missing data and high collinearity, we preprocess the data, leaving only around 20 features; see the appendix for details. Figure 3 reports the rank of the scores of the actual root causes.

6 Conclusion and Limitations

We introduce a simple yet effective approach for RCA in linear SEMs, which, to our knowledge, is the only method that provably works for unknown cyclic graphs using a simple anomalous sample. In addition, it remains applicable in the presence of multiple root causes or latent variables, given that the graph is sufficiently sparse. It relies crucially on the assumption that the SEM describing the normal regime also holds for the

anomalous regime. Whether this assumption holds depends heavily on the respective use case; we have shown a real-world example where the method at least clearly outperforms chance level. In simulation studies, our method outperforms existing approaches, while offering faster computation.

Acknowledgements

This project has received funding from the European Research Council (ERC) under the European Union’s Horizon 2020 research and innovation programme (grant agreement No 883818). DS acknowledges support by the DAAD program Konrad Zuse Schools of Excellence in Artificial Intelligence, sponsored by the Federal Ministry of Education and Research.

Bibliography

- Carlos Amendola, Philipp Dettling, Mathias Drton, Federica Onori, and Jun Wu. Structure learning for cyclic linear causal models. In Jonas Peters and David Sontag, editors, *Proceedings of the 36th Conference on Uncertainty in Artificial Intelligence (UAI)*, volume 124 of *Proceedings of Machine Learning Research*, pages 999–1008. PMLR, 03–06 Aug 2020.
- Charles K. Assaad, Imad Ez-Zejjari, and Lei Zan. Root cause identification for collective anomalies in time series given an acyclic summary causal graph with loops. In Francisco Ruiz, Jennifer Dy, and Jan-Willem van de Meent, editors, *Proceedings of the 26th International Conference on Artificial Intelligence and Statistics*, volume 206 of *Proceedings of Machine Learning Research*, pages 8395–8404. PMLR, 25–27 Apr 2023.
- Patrick Blöbaum, Peter Götz, Kailash Budhathoki, Atalanti A. Mastakouri, and Dominik Janzing. Dowhy-gcm: An extension of dowhy for causal inference in graphical causal models. *Journal of Machine Learning Research*, 25(147):1–7, 2024. URL <http://jmlr.org/papers/v25/22-1258.html>.
- Tobias Boege, Mathias Drton, Benjamin Hollering, Sarah Lump, Pratik Misra, and Daniela Schkoda. Conditional independence in stationary distributions of diffusions. *Stochastic Processes and their Applications*, 184:104604, 2025.
- Stephan Bongers, Patrick Forré, Jonas Peters, and Joris M. Mooij. Foundations of structural causal models with cycles and latent variables. *The Annals of Statistics*, 49(5):2885 – 2915, 2021.

- Philip Dawid. Decision-theoretic foundations for statistical causality. *Journal of Causal Inference*, 9(1): 39–77, 2021.
- Jerome Friedman, Trevor Hastie, and Robert Tibshirani. Sparse inverse covariance estimation with the graphical lasso. *Biostatistics*, 9(3):432–441, 2008.
- Patric Genfer and Uwe Zdun. Identifying domain-based cyclic dependencies in microservice APIs using source code detectors. In Stefan Biffl, Elena Navarro, Welf Löwe, Marjan Sirjani, Raffaella Mirandola, and Danny Weyns, editors, *Software Architecture*, pages 207–222, Cham, 2021. Springer International Publishing.
- Asish Ghoshal, Kevin Bello, and Jean Honorio. Direct learning with guarantees of the difference DAG between structural equation models. arXiv preprint arXiv:1906.12024, 2019.
- Peter Grünwald, Rianne de Heide, and Wouter Koolen. Safe testing. *Journal of the Royal Statistical Society Series B: Statistical Methodology*, 86(5):1091–1128, 03 2024.
- Michaela Hardt, William Roy Orchard, Patrick Blöbaum, Elke Kirschbaum, and Shiva Kaviswanathan. The petshop dataset — finding causes of performance issues across microservices. In *Proceedings of the Third Conference on Causal Learning and Reasoning (CLEaR)*, volume 236 of *Proceedings of Machine Learning Research*, pages 957–978. PMLR, 2024.
- Azam Ikram, Sarthak Chakraborty, Subrata Mitra, Shiv Kumar Saini, Saurabh Bagchi, and Murat Kocaoglu. Root cause analysis of failures in microservices through causal discovery. In *Advances in Neural Information Processing Systems*, 2022.
- Amin Jaber, Murat Kocaoglu, Karthikeyan Shanmugam, and Elias Bareinboim. Causal discovery from soft interventions with unknown targets: Characterization and learning. In H. Larochelle, M. Ranzato, R. Hadsell, M.F. Balcan, and H. Lin, editors, *Advances in Neural Information Processing Systems*, volume 33, pages 9551–9561. Curran Associates, Inc., 2020. URL https://proceedings.neurips.cc/paper_files/paper/2020/file/6cd9313ed34ef58bad3fdd504355e72c-Paper.pdf.
- Myunghwan Kim, Roshan Sumbaly, and Sam Shah. Root cause detection in a service-oriented architecture. In *Proceedings of the ACM SIGMETRICS/International Conference on Measurement and Modeling of Computer Systems*, SIGMETRICS '13, page 93–104, New York, NY, USA, 2013. Association for Computing Machinery.
- Murat Kocaoglu, Amin Jaber, Karthikeyan Shanmugam, and Elias Bareinboim. Characterization and learning of causal graphs with latent variables from soft interventions. In *Proceedings of the 33rd International Conference on Neural Information Processing Systems*, Red Hook, NY, USA, 2019. Curran Associates Inc.
- Jinzhou Li, Benjamin B. Chu, Ines F. Scheller, Julien Gagneur, and Marloes H. Maathuis. Root cause discovery via permutations and Cholesky decomposition, 2024. URL <https://arxiv.org/abs/2410.12151>.
- Vineet Malik, Kevin Bello, Asish Ghoshal, and Jean Honorio. Identifying causal changes between linear structural equation models. In Negar Kiyavash and Joris M. Mooij, editors, *Proceedings of the 40th Conference on Uncertainty in Artificial Intelligence*, volume 244 of *Proceedings of Machine Learning Research*, pages 2383–2398. PMLR, 15–19 Jul 2024.
- Joris M. Mooij, Sara Magliacane, and Tom Claassen. Joint causal inference from multiple contexts. *Journal of Machine Learning Research*, 21(99):1–108, 2020. URL <http://jmlr.org/papers/v21/17-123.html>.
- Nastaran Okati, Sergio Garrido Mejia, William Roy Orchard, Patrick Blöbaum, and Dominik Janzing. Root cause analysis of outliers with missing structural knowledge. In *Advances in Neural Information Processing Systems*, volume 39. Curran Associates, Inc., 2025. URL <https://neurips.cc/virtual/2025/poster/119709>.
- Thomas Richardson. A discovery algorithm for directed cyclic graphs. In *Proceedings of the Twelfth International Conference on Uncertainty in Artificial Intelligence*, UAI'96, page 454–461, San Francisco, CA, USA, 1996. Morgan Kaufmann Publishers Inc.
- J. Schur. Über Potenzreihen, die im Innern des Einheitskreises beschränkt sind. *Journal für die reine und angewandte Mathematik*, 147:205–232, 1917. URL <http://eudml.org/doc/149467>.
- Mohammad Reza Saleh Sedghpour, David Garlan, Bradley R. Schmerl, Cristian Klein, and Johan Tordsson. Breaking the vicious circle: Self-adaptive microservice circuit breaking and retry. In *IC2E*, pages 32–42, 2023.
- Huasong Shan, Yuan Chen, Haifeng Liu, Yunpeng Zhang, Xiao Xiao, Xiaofeng He, Min Li, and Wei Ding. ϵ -diagnosis: Unsupervised and real-time diagnosis of small-window long-tail latency in large-scale microservice platforms. In *Proceedings of The World Wide Web Conference*, pages 3215–3222, New York, NY, USA, 2019. Association for Computing Machinery.

- Amit Sharma and Emre Kiciman. Dowhy: An end-to-end library for causal inference. *arXiv preprint arXiv:2011.04216*, 2020.
- Peter Spirtes, Clark Glymour, and Richard Scheines. *Causation, Prediction, and Search*. The MIT Press, 01 2001.
- Hongyuan Tao, Hang Yu, and Jianguo Li. DeepITE: Designing variational graph autoencoders for intervention target estimation. In A. Globerson, L. Mackey, D. Belgrave, A. Fan, U. Paquet, J. Tomczak, and C. Zhang, editors, *Advances in Neural Information Processing Systems*, volume 37, pages 89978–90008. Curran Associates, Inc., 2024.
- Andrea Tonon, Meng Zhang, Bora Caglayan, Fei Shen, Tong Gui, MingXue Wang, and Rong Zhou. RADICE: Causal graph based root cause analysis for system performance diagnostic. In *2025 IEEE International Conference on Software Analysis, Evolution and Reengineering (SANER)*, pages 465–475, 2025. doi: 10.1109/SANER64311.2025.00050.
- Burak Varici, Karthikeyan Shanmugam, Prasanna Sattigeri, and Ali Tajer. Scalable intervention target estimation in linear models. In M. Ranzato, A. Beygelzimer, Y. Dauphin, P.S. Liang, and J. Wortman Vaughan, editors, *Advances in Neural Information Processing Systems*, volume 34, pages 1494–1505. Curran Associates, Inc., 2021.
- Burak Varici, Karthikeyan Shanmugam, Prasanna Sattigeri, and Ali Tajer. Intervention target estimation in the presence of latent variables. In James Cussens and Kun Zhang, editors, *Proceedings of the Thirty-Eighth Conference on Uncertainty in Artificial Intelligence*, volume 180 of *Proceedings of Machine Learning Research*, pages 2013–2023. PMLR, 01–05 Aug 2022.
- Julius Von Kügelgen, Abdirisak Mohamed, and Sander Beckers. Backtracking counterfactuals. In Mihaela van der Schaar, Cheng Zhang, and Dominik Janzing, editors, *Proceedings of the Second Conference on Causal Learning and Reasoning*, volume 213 of *Proceedings of Machine Learning Research*, pages 177–196. PMLR, 11–14 Apr 2023.
- Vladimir Vovk and Ruodu Wang. E-values: Calibration, combination and applications. *The Annals of Statistics*, 49(3):1736 – 1754, 2021.
- Ruodu Wang and Aaditya Ramdas. False discovery rate control with e-values. *Journal of the Royal Statistical Society Series B: Statistical Methodology*, 84(3):822–852, 01 2022.
- Yuhao Wang, Chandler Squires, Anastasiya Belyaeva, and Caroline Uhler. Direct estimation of differences in causal graphs. In S. Bengio, H. Wallach, H. Larochelle, K. Grauman, N. Cesa-Bianchi, and R. Garnett, editors, *Advances in Neural Information Processing Systems*, volume 31. Curran Associates, Inc., 2018. URL <https://proceedings.neurips.cc/paper/2018/file/e1314fc026da60d837353d20aefaf054-Paper.pdf>.
- Zhiqiang Xie, Yujia Zheng, Lizi Ottens, Kun Zhang, Christos Kozyrakis, and Jonathan Mace. Cloud atlas: Efficient fault localization for cloud systems using language models and causal insight, 2024. URL <https://arxiv.org/abs/2407.08694>.
- Yuqin Yang, Saber Salehkaleybar, and Negar Kiyavash. Learning unknown intervention targets in structural causal models from heterogeneous data. In Sanjoy Dasgupta, Stephan Mandt, and Yingzhen Li, editors, *Proceedings of The 27th International Conference on Artificial Intelligence and Statistics*, volume 238 of *Proceedings of Machine Learning Research*, pages 3187–3195. PMLR, 02–04 May 2024.

Supplementary Material

A Missing Proofs and Details on Genericity Assumptions

A.1 Proof of Lemma 2.1

We begin by expressing the inverse in terms of the adjugate:

$$((I - A)^{-1})_{ij} = \frac{1}{\det(I - A)} (\text{adj}(I - A))_{ij}.$$

To expand the adjugate entry $\text{adj}(I - A)_{ij}$, fix i and j , and let $I - \tilde{A}$ the matrix obtained from $I - A$ by setting all entries in column i and row j to zero, except $(I - \tilde{A})_{ji}$, which is set to 1. Then, by Leibniz-Expansion,

$$(\text{adj}(I - A))_{ij} = \det(I - \tilde{A}) = \sum_{\sigma \in S_p} \left(\text{sgn}(\sigma) \prod_{m=1}^p (I - \tilde{A})_{m, \sigma(m)} \right) \quad (7)$$

Note that any permutation can be decomposed into disjoint cyclic components⁴, say $\sigma = C_1 \circ \dots \circ C_s$. These components can be understood as graphical cycles: The matrix $I - \tilde{A}$ is the adjacency matrix of the graph \tilde{G} constructed from G with these modifications:

1. Remove all incoming edges to node j and all outgoing edges from node i .
2. Multiply all edge weights by -1 .
3. Add self-loops at each node except for i, j .
4. Add a single edge $i \rightarrow j$ with weight 1.

In (7), the summand for a permutation $\sigma \in S_n$ is non-zero only if for all k , the edge $k \rightarrow \sigma(k)$ exists in \tilde{G} . Therefore, we restrict to these permutations henceforth. For such a permutation σ , each cyclic component $\sigma(i_1) = i_2, \sigma(i_2) = i_3, \dots, \sigma(i_{k-1}) = i_k, \sigma(i_k) = i_1$ corresponds to the cycle $i_1 \rightarrow i_k \rightarrow i_{k-1} \rightarrow \dots \rightarrow i_2 \rightarrow i_1 \in \tilde{G}$. Also the sign of the permutation can be decomposed according to the cycles: $\text{sgn}(\sigma) = (-1)^{p-s} = (-1)^{l_1 + \dots + l_s - s}$, l_s being the lengths of the cycles. Combined, this leads to

$$(\text{adj}(I - A))_{ij} = \sum_{\substack{(C_1, \dots, C_s): \text{ disjoint cycles} \\ \text{in } \tilde{G} \text{ covering all nodes } [p]}} (-1)^s \prod_{m=1}^s (-1)^{l_m} \prod_{k \rightarrow h \in C_m} (I - \tilde{A})_{hk}. \quad (8)$$

To relate this back to G , we go through the differences with \tilde{G} . Fix a permutation $\sigma = C_1 \circ \dots \circ C_s$ contributing a non-zero summand. First note that due to 1. and 4. the only outgoing edge of j leads to i , so $\sigma(j) = i$; otherwise the corresponding summand would be 0. In graphical terms, this means $i \rightarrow j$ is in one of the cycles, lets say in C_s . Because of 4., $i \rightarrow j$ is not necessarily in G . However, it has anyways weight 1 in \tilde{G} , so we may omit this factor in the product; in formulas

$$(-1)^{l_s} \prod_{h \rightarrow k \in C_s} (I - \tilde{A})_{hk} = (-1)^{l_s + 1} \prod_{h \rightarrow k \in \pi} (I - \tilde{A})_{hk}$$

⁴A cyclic component of a permutation $\sigma \in S_n$ is a sequence of distinct elements $C = (i_1 \ i_2 \ \dots \ i_k)$ such that $\sigma(i_1) = i_2, \sigma(i_2) = i_3, \dots, \sigma(i_{k-1}) = i_k, \sigma(i_k) = i_1$. It can be viewed as an element of S_n by defining $C(j) = j$ for all $j \in [p] \setminus \{i_1, \dots, i_k\}$. Using this extension, one obtains that σ is the product of all its cyclic components.

where π is the path $j \rightsquigarrow i$ obtained from C_s by dropping $i \rightarrow j$, and l_π its length. Note that π does not feature any self-loops, since the cyclic component C_s consists of distinct elements. Therefore, $\pi \in G$, and the expression further simplifies to

$$\begin{aligned} (-1)^{l_\pi+1} \prod_{h \rightarrow k \in \pi} (I - \tilde{A})_{hk} &\stackrel{h \neq k}{=} (-1)^{l_\pi} \prod_{k \rightarrow h \in \pi} (\tilde{A})_{hk} \\ &\stackrel{2.}{=} (-1)^{l_\pi+1} \prod_{k \rightarrow h \in \pi} -a_{hk} \\ &= - \prod_{k \rightarrow h \in \pi} a_{hk}. \end{aligned} \tag{9}$$

Analogously, for every cycle neither using $i \rightarrow j$ nor self-loops,

$$(-1)^{l_m} \prod_{k \rightarrow h \in C_m} (I - \tilde{A})_{hk} = \prod_{k \rightarrow h \in C} a_{hk}.$$

Finally, some of the cycles might be self-loops, lets say C_1, \dots, C_r . Again, they have edge weight 1, and also the signs $(-1)^r \cdot \prod_{m=1}^r (-1)^{l_m} = 1$ cancel out, so we may omit them from the product in (8). This omission is reflected in the overall sum by no longer requiring that $(C_1, \dots, C_{s-1}, \pi)$ together cover all nodes. More precisely, define $\mathcal{C}_\pi = \{(C_1, \dots, C_q) : \text{collection of disjoint cycles in } \tilde{G} \text{ not using any node in } \pi; q \in \mathbb{N}_0\}$. Then,

$$(\text{adj}(I - A))_{ij} = - \sum_{\pi: j \rightsquigarrow i} \prod_{k \rightarrow h \in \pi} a_{hk} \cdot \left(\sum_{(C_1, \dots, C_q) \in \mathcal{C}_\pi} (-1)^{q+1} \prod_{m=1}^q \prod_{k \rightarrow h \in C_q} a_{hk} \right).$$

In this expression, the term $(-1)^s$ in (8) becomes $(-1)^{q+1}$ since π is extracted from the overall sum, therefore not counted by q . Multiplying with -1 and moving the summand for $q = 0$ outside of the sum, we obtain the formula stated in the lemma:

$$((I - A)^{-1})_{ij} = \frac{1}{\det(I - A)} \sum_{\pi: j \rightsquigarrow i} \prod_{k \rightarrow h \in \pi} a_{hk} \cdot \left(1 + \sum_{\substack{(C_1, \dots, C_q) \in \mathcal{C}_\pi, \\ q \geq 1}} (-1)^q \prod_{m=1}^q \prod_{k \rightarrow h \in C_q} a_{hk} \right).$$

A.2 Proof of Theorem 3.1

As shown in Equation (4) in the main paper, $\xi \stackrel{d}{=} \Xi + ((I - A)^T \Theta_{NN} \Delta)$, implying that $\xi_i \stackrel{d}{\neq} \Xi_i$ if and only if $((I - A)^T \Theta_{NN} \Delta)_i \neq 0$. Using that Δ is non-zero only at the root cause positions, we obtain

$$((I - A)^T \Theta_{NN} \Delta)_i = (I - A)_{:,i} \Theta_{NN} \Delta = \sum_{r \in \mathcal{R}} (I - A)_{r,i} \sigma_r^{-2} \delta_r = \sigma_i^{-2} \delta_i - \sum_{r \in \mathcal{R} \cap \text{pa}(i)} a_{r,i} \sigma_r^{-2} \delta_r,$$

which is generically non-zero for all nodes except the root causes and their parents, and definitively zero for all other nodes. The exceptional parameter set on which $\xi_r \stackrel{d}{=} \Xi_r$ for some root cause r can be directly read off from the above equation: it consists of all parameter choices $a_{ij}, \sigma_{N_i}, \delta_i$ for which, for any root cause $r \in \mathcal{R}$,

$$((I - A)^T \Theta_{NN} \Delta)_r = 0.$$

That is, when the causal model is applied to Δ , the perturbations cancel exactly. This situation only arises if there are multiple root causes that are directly linked in the graph for a measure zero set of choices for all non-zero $a_{ij}, \sigma_{N_i}, \delta_i$.

A.3 Proof of Theorem 3.2

The claim follows directly from Theorem 3.1 together with the observation that root causes and their descendants are generically anomalous, i.e., $\tilde{x}_r \stackrel{d}{\neq} X_r$, while for all other nodes $\tilde{x}_i \stackrel{d}{=} X_i$. The exceptional set is the union of that from Theorem 3.1 and all parameter choices for which even a root cause is not anomalous, namely those satisfying

$$0 = ((I - A)^{-1} \Delta)_r.$$

Again, this can only happen if there are multiple directly connected root causes.

A.4 Proof of Lemma 3.4

Assume first that the noise vector N is jointly Gaussian, then $\bar{N} = N_X + (I - A)_{XL}(I - A_{LL})^{-1}N_L$ is also Gaussian, and the sparsity pattern of the precision matrix $K_{\bar{N}} := \Sigma_{\bar{N}}^{-1}$ corresponds to conditional independence relations among the components of \bar{N} . In particular, we have

$$(K_{\bar{N}})_{ij} = 0 \Leftrightarrow \bar{N}_i \perp\!\!\!\perp \bar{N}_j \mid N_{[p] \setminus \{i,j\}}.$$

Denoting $B = (I - A)_{XL}(I - A_{LL})^{-1}$, we observe that \bar{N} combined with N_L fulfills the linear SEM

$$\begin{pmatrix} \bar{N} \\ N_L \end{pmatrix} = \begin{pmatrix} 0 & B \\ 0 & 0 \end{pmatrix} \begin{pmatrix} \bar{N} \\ N_L \end{pmatrix} + \begin{pmatrix} N_X \\ N_L \end{pmatrix} \quad (10)$$

Conditional independencies among the components of \bar{N} then follow from d-separation in the corresponding graph. Specifically, $\bar{N}_i \perp\!\!\!\perp \bar{N}_j \mid N_{[p] \setminus \{i,j\}}$ is equivalent to \bar{N}_i and \bar{N}_j being d-connected given \bar{N} . Since the SEM (10) only features edges from N_L to \bar{N} this further breaks down to the existence of a path $\bar{N}_i \leftarrow N_{L_{l_1}} \rightarrow \bar{N}_{i_1} \leftarrow N_{L_{l_2}} \rightarrow \dots \rightarrow \bar{N}_j$. Since $B = A_{XL}(I - A_{LL})^{-1}$ and $(I - A_{LL})^{-1}$ encodes directed paths using only latents, $B_{il} \neq 0$ whenever in the graph belonging to \mathcal{Z} , there is a path from l to i using just latents. Combining both, the statement of the lemma follows.

Turning to general distributions, note that $K_{\bar{N}} = (\Sigma_{N_X} + B^T \Sigma_{N_L} B)^{-1}$ which depends only on the covariance of N and no other properties of the distribution. Thus, the lemma holds for arbitrary distributions of N .

A.5 Proof of Theorem 3.5

The deviation in the paper already proves that the theorem holds generically. The exception set can be obtained analogously to the one of Theorem 3.1. Specifically, $\xi_r \stackrel{d}{=} \Xi_r$ for an observable root cause r if

$$0 \neq ((I - \bar{A})^T \Theta_{\bar{N}\bar{N}} \bar{\Delta})_r.$$

B Other Perspectives on Our Score

Relation to Linear Regression As mentioned in the main paper, there are two other interpretations of our score $s = \text{Z-score}(\xi; \Xi)$ worth mentioning. The first one is that it relates to linear regression. Specifically, consider the linear regression model

$$X_j = \sum_{i \neq j} \alpha_i X_i + E_j$$

with the data from the normal regime X as the training data set, i.e. the coefficients are learned by fitting on this distribution. Under infinite sample size this yields

$$\alpha_i = -\frac{\Theta_{ji}}{\Theta_{jj}} \quad (i \neq j),$$

and a residual with constant variance

$$\text{Var}(E_j) = \frac{1}{\Theta_{jj}}.$$

Next, testing the model on the anormal sample \tilde{x}_j , we obtain the residual

$$\tilde{e}_j = \tilde{x}_j - \sum_{i \neq j} \alpha_i \tilde{x}_i = \tilde{x}_j + \sum_{i \neq j} \frac{\Theta_{ji}}{\Theta_{jj}} \tilde{x}_i = \frac{1}{\Theta_{jj}} (\Theta \tilde{x}) = \frac{1}{\Theta_{jj}} \xi. \quad (11)$$

Combining this with $\text{Var}(\Xi) = \Theta$ so that $\text{Z-score}(\xi_j; \Xi_j) = (\Theta \tilde{x})_j / \sqrt{\Theta_{jj}}$, yields the following result.

Lemma B.1. *Let E_j the residual of the linear equation model predicting X_j in terms of X_{-j} and \tilde{e}_j the residual when testing the model on \tilde{x}_j as defined in (11). Then,*

$$\text{Z-score}(\xi_j; \Xi_j) = \frac{\tilde{e}_j}{\text{std}(E_j)}.$$

Assuming X to be Gaussian this further simplifies: In this case, the linear predictor coincides with the conditional mean, that is

$$\mathbb{E}(X_j | X_{-j} = \tilde{x}_{-j}) = \sum_{i \neq j} \alpha_i \tilde{x}_i.$$

Moreover, the conditional variance is the residual’s variance: $\text{Var}(X_j | X_{-j} = \tilde{x}_{-j}) = \text{Var}(E_j)$. Therefore, the Z-score($\xi_j; \Xi_j$) can also be seen as a conditional Z-score of \tilde{x} :

$$\text{Z-score}(\xi_j; \Xi_j) = \text{Z-score}(\tilde{x}_j; X_j | X_{-j} = \tilde{x}_{-j}) := \frac{|\tilde{x}_j - \mathbb{E}(X_j | X_{-j} = \tilde{x}_{-j})|}{\text{Var}(X_j | X_{-j} = \tilde{x}_{-j})^{1/2}}.$$

RCA via Conditional Independence Testing Many existing RCA or intervention target estimation approaches rely on conditional independence testing (Kocaoglu et al., 2019; Jaber et al., 2020; Mooij et al., 2020; Ikram et al., 2022). To see that we first need to introduce a different perspective on modelling perturbations on root causes. For simplicity, we present it for the case of one root cause, but the approach can also be done for multiple ones. Specifically, one combines the normal and anomalous datasets $\mathbf{X} \in \mathbb{R}^{m \times p}$, $\tilde{\mathbf{x}} \in \mathbb{R}^{1 \times p}$ into one joint dataset $\mathbf{Y} \in \mathbb{R}^{(m+1) \times (p+1)}$ by introducing a ‘regime indicator’ (Dawid, 2021)⁵ variable F , that is, a binary feature indicating whether a sample is anormal or normal:

$$\mathbf{Y} = \begin{pmatrix} X^{(1)} & 0 \\ \vdots & \vdots \\ X^{(m)} & 0 \\ \tilde{x} & 1 \end{pmatrix}$$

One can then show that the corresponding P^Y satisfies again linear SEM, specifically the equations for all non-root cause features remain the same, while

$$Y_r = \sum_{Y_i \in \text{pa}(i) \setminus \{F\}} a_{ri} Y_i + \delta F + \epsilon_r$$

$$F = \epsilon_0 \sim \text{Bernoulli}\left(\frac{m_2}{m + m_2}\right).$$

So, the corresponding graph is the same as G with one additional node F and an edge $F \rightarrow Y_r$. Note that this model also works without assuming linear dependencies, letting each node be any function of its parents and noise term. In both cases, the Markov property of the graph yields

$$Y_j \perp\!\!\!\perp F | Y_{-j} \iff Y_j \notin \text{pa}(Y_r) \cup \{Y_r\}, \quad (12)$$

which again reveals the root cause and its parents. Now since F is binary, testing this independence is the same as assessing whether the two distributions where $F = 0, 1$, respectively, are the same:

$$H_0 : X_j | X_{-j} \sim \tilde{x}_j | \tilde{x}_{-j};$$

compare Definition 2 in Jaber et al. (2020). Both our Z-Score(ξ_i, Ξ_i) as well as the conditional Z-score can be seen as test statistics for this hypothesis, as they become 0 under H_0 . However, without any parametric assumptions, estimating the conditional Z-score is complex, and for both scores, without any assumptions, it is involved to derive the null distribution and assess the power. In contrast, as demonstrated in the main paper, under a linear SEM and for sufficiently large intervention strength δ , our test has statistical power even with a single anomalous sample. This reliance on just one anomalous sample constitutes the key distinction between our approach and other conditional independence–based RCA methods. For instance, while Jaber et al. (2020) also employs the test in (12) (among others), they do not provide a practical algorithm and establish guarantees only under the assumption of an oracle CI test. Nonetheless, since (12) also holds in the nonlinear case, this viewpoint may serve as a starting point for developing a generalization of our method for nonlinear data.

⁵Also called ‘F-node’ (Jaber et al., 2020) or ‘context variable’ in the literature (Mooij et al., 2020).

C Cholesky Decomposition-Based RCA and Its Relation to Our Method

The method of Li et al. (2024) assumes G to be a DAG and then identifies the root cause as follows: Like our approach, they start with the fact that under the linear SEM,

$$\Sigma_{XX} = (I - A)^{-1}\Sigma_{NN}(I - A)^{-T}.$$

Their core idea is that if X is arranged according to a topological order of the DAG, then $I - A$ is lower triangular. Therefore, also the product $L = (I - A)^{-1}\Sigma_{NN}^{1/2}$ is lower triangular and can be recovered from Σ_{XX} : Specifically, L is the so-called Cholesky factor of Σ_{XX} , defined as the lower triangular matrix satisfying $LL^T = \Sigma_{XX}$, which is unique and can be computed from Σ_{XX} . Knowing L , we can recover the noise up to standardization: Since $X = (I - A)^{-1}N$,

$$N_{\text{std}} = \left((I - A)^{-1}\Sigma_{NN}^{1/2} \right)^{-1} X$$

where N_{std} is the standardized version of N . Similarly, the perturbed noise can be recovered (up to rescaling with the normal noise’s variance) as $\Sigma_{NN}^{-1/2}\tilde{n}_{\text{std}} = L^{-1}\tilde{x}$, whose only extreme entry directly identifies the root cause.

Because the correct ordering is not known, their method iterates over all permutations π , computing the Cholesky factor L_π of the permuted covariance and checking whether $L_\pi^{-1}\tilde{x}$ has exactly one extreme value. Based on non-trivial linear algebra insights, they show that as soon as they found one π yielding precisely one extreme component i , then i is indeed the root cause. Such a π does not necessarily represent the true causal ordering; instead it must locally respect the structure around i insofar as the parents of i precede i , and its descendants appear after.

To compare their method to ours, note that we obtain a sparse vector via applying the transformation Θ_{XX} to the observed vector \tilde{x} , while they get a sparse vector via applying L_π^{-1} to \tilde{x} . Their method is more accurate in the sense that $L_\pi^{-1}\tilde{x}$ is only extreme for the root cause, while $\Theta_{XX}\tilde{x}$ only identifies a short list of root causes. However, in the acyclic case, by intersecting with the nodes that are actually anomalous, we also obtain the unique root cause; compare Theorem 3.2.

D Further Details on Experiments

D.1 Choice of Hyperparameters

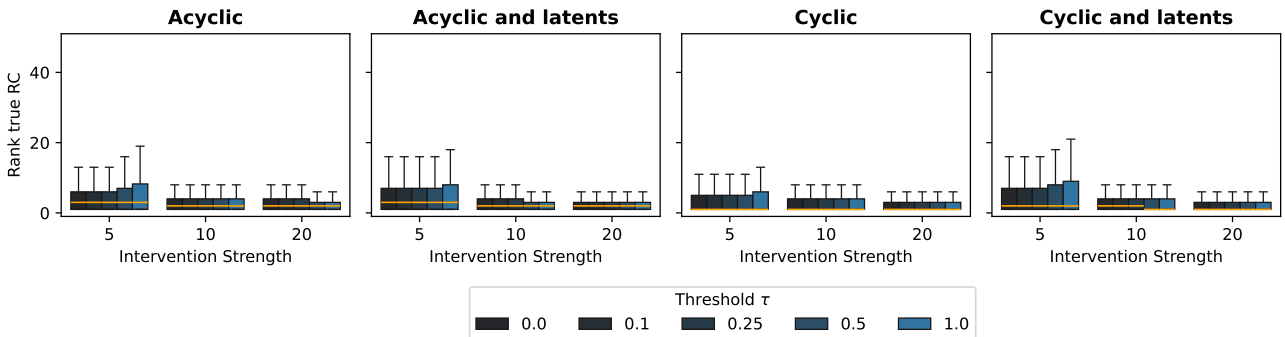


Figure 4: Effect of the threshold parameter τ on RCA performance for different intervention strengths when using Cyclic (Graphical Lasso) on 50 nodes with the same data simulation setup as in the main paper. The weaker the interventions, the lower τ values are preferable.

Our method involves two hyperparameters: the threshold τ that distinguishes normal from anomalous features, and the regularization parameter α in the Graphical Lasso. A suitable choice of τ can be expected to depend on the strength of the intervention. Indeed, as shown in Figure 4, for lower intervention strengths it is beneficial to select a smaller τ . This reflects the fact that an intervention strength of 5 only induces mild anomalies, since 5 is quite small compared to the noise variance in our simulation setup (for instance, for Gaussian noise, we sample

the standard deviation of each noise term uniformly sampled from $[0.5, 2]$). For our simulation studies, we set $\tau = 0.25$ to achieve reliable performance already at small intervention strengths. In practical applications, this threshold has the advantage of being intuitively interpretable: domain experts can often set it based on their expectation of how anomalous the data should appear in a given scenario. Otherwise, we recommend selecting τ after inspecting the anomaly scores of all features, potentially revealing to clusters of normal versus anomalous features.

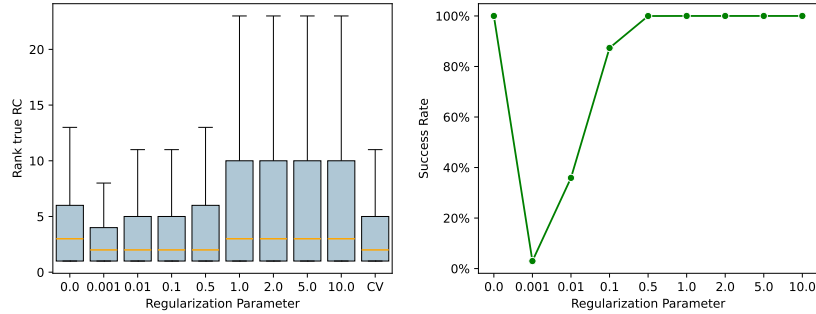


Figure 5: Left: Performance of Cyclic (Graphical) across different regularization parameters α in the Graphical Lasso. The data are generated as described in the main paper, but here all graph types and intervention strengths are combined into a single plot. Note that the Graphical Lasso may fail for small α , since the regularization is insufficient to stabilize inversion of ill-conditioned matrices. Only successful replications are included here. ‘CV’ denotes selection of α via cross-validation. Right: Corresponding success rate of Graphical Lasso.

Regarding the regularization parameter α , Figure 5 (left) shows that the best results are obtained for $\alpha = 0.001$. However, as seen in the right plot, Graphical Lasso frequently fails due to instability for such small α values. Therefore, we initialize with $\alpha = 0.1$ and increase it by a factor of 10 in case of failure. If the method still fails after two such increases, our implementation defaults to using the inverse covariance matrix instead. In practice, this fallback was never required in our experiments. Another possible strategy to ensure success is to select α via cross-validation. While this approach is computationally more expensive, it achieves performance comparable to that obtained with $\alpha = 0.1$, as shown in the rightmost column of Figure 5 (left).

D.2 Precision Estimation

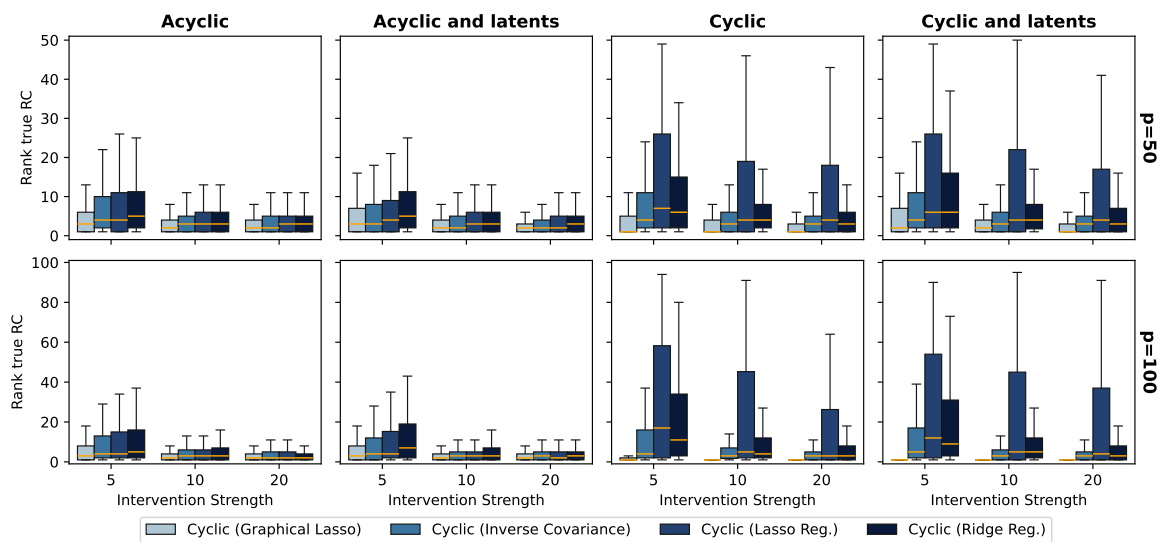


Figure 6: Ranks of the actual root causes under the same simulation settings as in Figure 2. The Lasso and Ridge regression variants both significantly underperform the methods presented in the main paper.

A challenge in both methods is the need to estimate the inverse of the covariance matrix (our method) or its Cholesky factor (Cholesky method), which might be ill-conditioned. While stronger regularization can alleviate this issue as shown above, it may not resolve cases such as almost-perfect feature correlation, which shows up in our real-data experiment. In this case, we recommend applying PCA to merge such highly correlated features; compare Section D.4. While this merging may combine the root cause with other features, potentially obscuring its identity, we argue that if the root cause r is strongly correlated with another feature r' , it becomes inherently difficult to distinguish between the two based on data alone. Thus, treating them as a single node is justifiable.

Even after mitigating high correlations, precision matrix estimation remains challenging and poses not only the computational but also the statistical bottleneck of our method. Therefore, in addition to the Graphical Lasso and inverting the sample covariance approaches described in the main paper, we explored alternative strategies. More specifically, we tried to bypass precision estimation entirely by first estimating the sample covariance matrix, and then solving $\hat{\Sigma}\hat{\xi} = \hat{x}$ using Lasso or Ridge Regression with regularization parameter 10^{-4} . In both cases, the baseline Ξ is not estimated, and the scores s_i in line 5 of the algorithm are simply set to $|\hat{\xi}_i|$. However, as Figure 6 illustrates, both alternatives perform worse than Graphical Lasso. The variance of the Lasso regression approach is particularly high. A likely reason is that Lasso enforces sparsity in its solutions. This means that if a the root cause’s score ξ_r is incorrectly shrunk to zero, the corresponding root cause will be assigned the lowest possible score (i.e., 0), which is a severe misclassification. In contrast, if the other methods make statistical errors, these are less likely to produce the extreme outcome of assigning score 0 to the true root cause.

D.3 Further Simulation Studies

Results broken down by different noise distributions. Figure 7 shows the results of same the simulation study as in the main paper for $p = 50$ but with performance metrics reported separately for each noise distribution choice.

Results broken down by different numbers of root cause. Figure 8 again visualizes the results as in the main paper for $p = 50$ but broken down by how many root causes are chosen.

Varying the expected degree. We expect the performance of both our methods as well as the Z-score baseline to depend heavily on the expected degree of the nodes: The higher the connectivity, the more nodes get infected by the root cause, are therefore anomalous, and have a high Z-score. In addition, the increased connectivity raises the probability that a node is a parent and descendants of the true root cause at the same time, thereby appearing in the shortlist described in Theorem 3.2. Indeed, the performance declines with higher degree as illustrated in Figure 9.

D.4 More details on Real-World Experiment

Preprocessing The PetShop dataset (Hardt et al., 2024) is organized with a three-level feature hierarchy in each CSV file: the top level corresponds to service names, the second to three core metrics (error rate, availability, and latency) and the third to statistical summaries used to aggregate these metrics over five-minute intervals (e.g., average, sum, and various percentiles). To reduce the data to the service level, we follow the PetShop package’s recommendation to select only one relevant metric per incident, based on the nature of the incident. Furthermore, since the “average” statistic is the only one consistently available across all services, we restrict to this statistic.

After this filtering, we remove any features that are either constant or exact duplicates of others, as these provide no additional information. We then discard columns with a high proportion of missing values and afterwards remove any rows that still contain NaNs. To normalize the features, we apply a robust standardization, which scales both normal and anomalous data using the mean and standard deviation computed solely from the normal operation period.

Finally, we apply service-level dimensionality reduction using Principal Component Analysis (PCA). This step identifies and merges highly correlated services, retaining the principal components that explain at least 90% of the variance. Doing so, we mitigate the presence of highly correlated features, which would otherwise lead to numerical instability in estimating the precision.

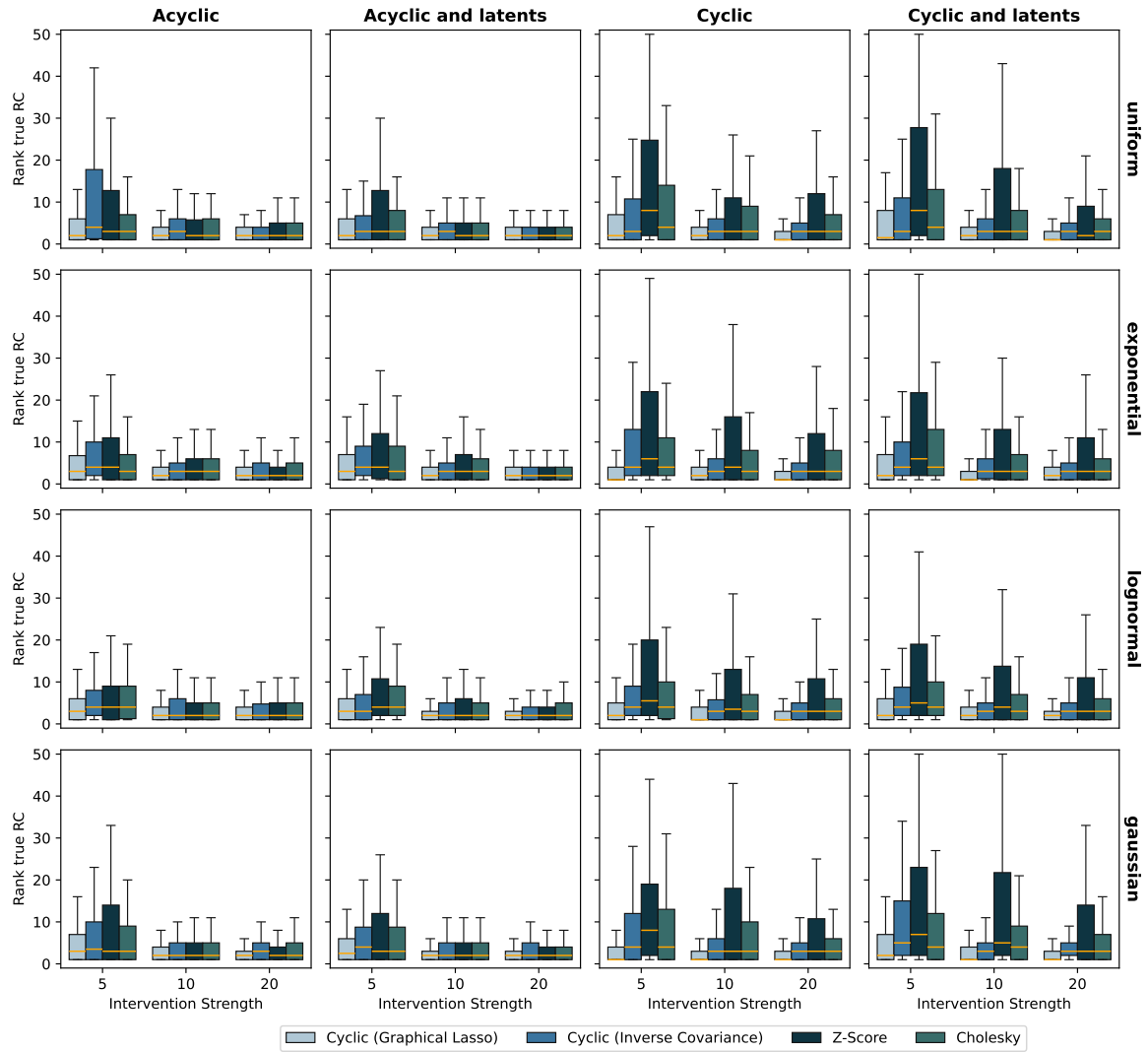


Figure 7: Performance for $p = 50$ across different noise distributions. All methods perform slightly weaker under uniform noise and $\delta = 5$, whereas for the other noise types and intervention strengths, no consistent patterns emerge.

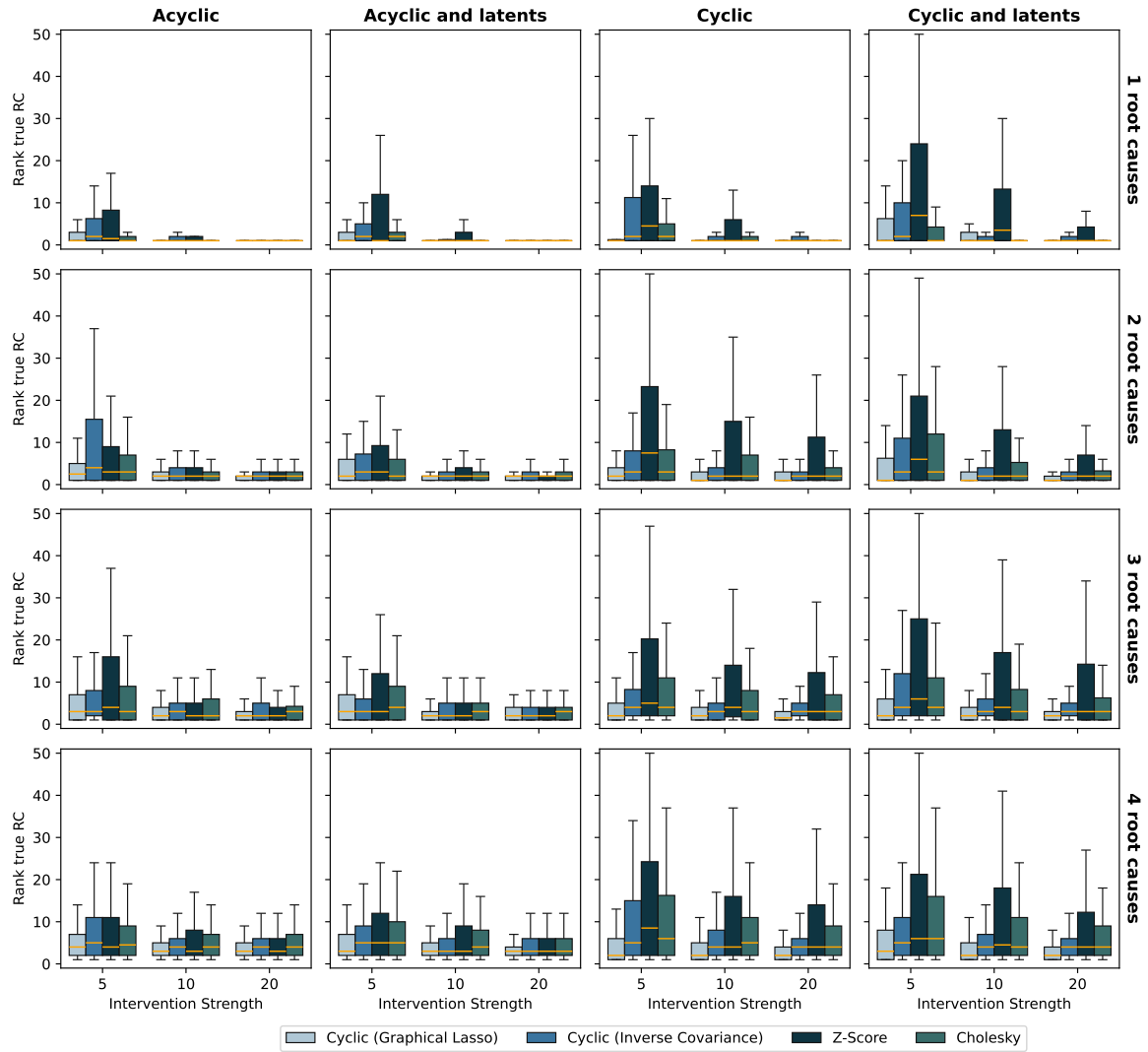


Figure 8: Performance for $p = 50$ when selecting 1, 2, 3 or 4 root causes. Unsurprisingly, performance decreases as the number of root causes increases, with the largest decline observed for Cholesky, which is designed to identify only a single root cause.

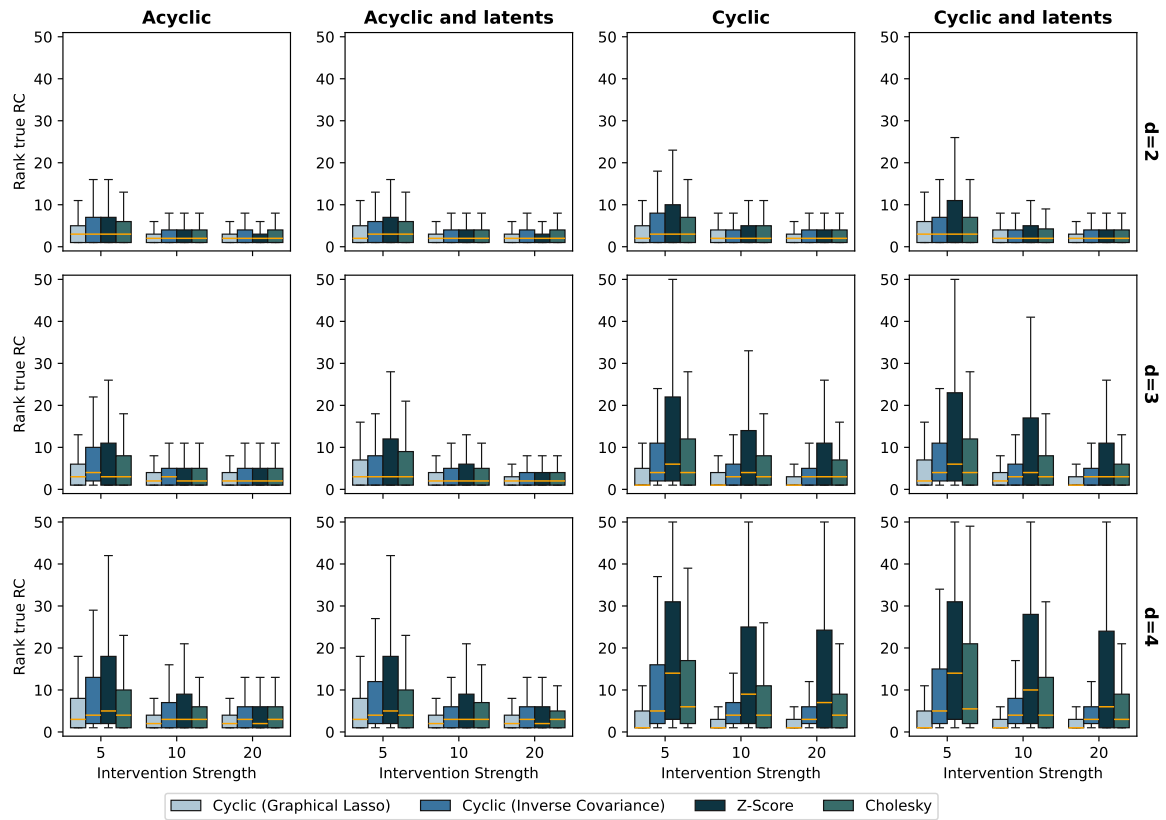


Figure 9: Performance at $p = 50$ across varying expected node degrees. All methods exhibit decreased performance as edge degree increases. This decline is minimal for Cyclic (Graphical Lasso), slightly more pronounced for Cyclic (Inverse Covariance) and Cholesky, and markedly strong for Z-score.

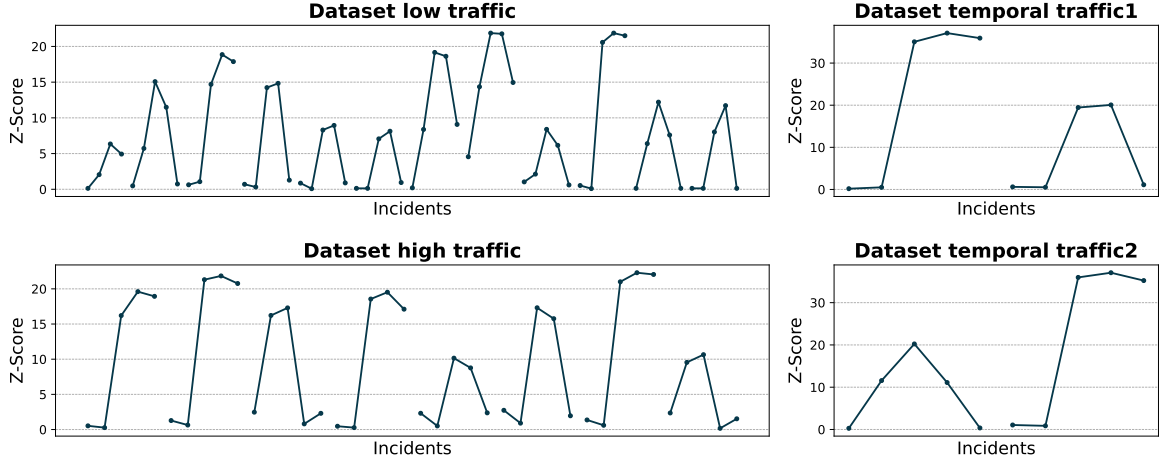


Figure 10: Z-scores of the actual root causes. Each line corresponds to one incident, with dots marking individual time points. The Z-scores tend to be close to 0 at the start and end, in stark contrast to the much higher values at intermediate time points.

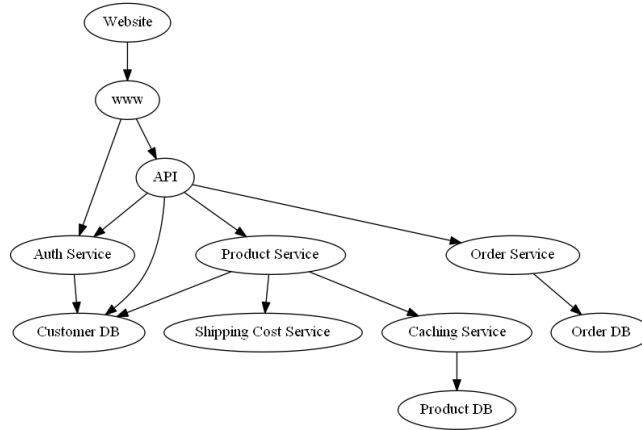


Figure 11: Microservice architecture underlying the semisynthetic dataset. Figure taken from DoWhy documentation.

Z-scores of the root causes As mentioned in the main paper, at both the start and end of each incident, the actual root causes tend not to show anomalous behavior. This is likely due to time delays between when an incident is triggered, and its effects become visible in the system. Moreover, at the end, the incident might already be resolved. Figure 10 illustrates this by plotting the absolute Z-scores (not ranks) of the actual root cause at all time points marked as anomalous in the data set.

D.5 Nonlinear Data

Finally, we evaluate our approach using a semisynthetic dataset derived from a case study in the DoWhy package (Sharma and Kiciman, 2020; Blöbaum et al., 2024). The dataset is produced by a structural equation model featuring primarily linear but also some nonlinear relationships, designed to resemble patterns typical of microservice data. More specifically, the data is generated according to the graph shown in Figure 11 and each X_i is the sum of its parents plus a noise term, with the following two exceptions:

$$X_{\text{Caching Service}} = Z \cdot X_{\text{Product DB}} + \epsilon_{\text{Caching Service}}, \text{ with } Z \sim \text{Bernoulli}(p = 0.5);$$

$$X_{\text{Product Service}} = \max(X_{\text{Shipping Cost Service}}, X_{\text{Caching Service}}, X_{\text{Customer DB}}) + \epsilon_{\text{Product Service}}$$

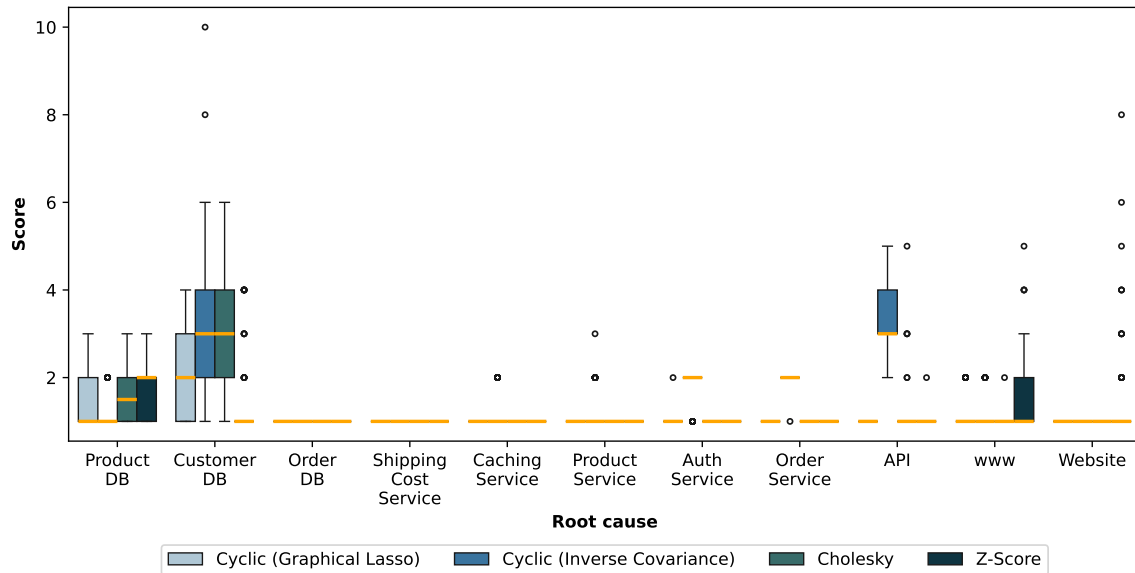


Figure 12: Root cause ranks across 100 replications, with the x-axis indicating the target node. Most methods place the true root cause in the top two, except for Cyclic (Inverse Covariance) and Cholesky on Customer DB and Cyclic (Inverse Covariance) on API.

For the noise distributions, truncated exponential noise (bounded above) is used for *Website*, *www*, *Order DB*, *Customer DB*, and *Product DB*, with varying truncation levels and a common scale parameter of 0.2. Half-normal noise (non-negative) is used for *API*, *Auth Service*, *Product Service*, *Order Service*, *Shipping Cost Service*, and *Caching Service*, with varying means and standard deviations.

In the original case study, the root cause is fixed as the *Caching Service*, perturbed by a shift of 2. By contrast, we extend this setup by conducting a series of experiments — one for every node as the root cause, which we also model by a shift intervention of 2. The RCA methods are then applied to the resulting data. Figure 12 shows that most methods rank the true root cause among the top two nodes, except for Cyclic (Inverse Covariance) and Cholesky performing worse when *Customer DB* is the root cause, and the Cyclic (Inverse Covariance) method drops in performance when intervening on *API*.